

RESEARCH

Open Access



# Salt weathering impact on Nero/Ramses II Temple at El-Ashmonein archaeological site (Hermopolis Magna), Egypt

Abdelrhman Fahmy<sup>1,2\*</sup>, Eduardo Molina-Piernas<sup>1</sup>, Javier Martínez-López<sup>1</sup> and Salvador Domínguez-Bella<sup>1</sup>

## Abstract

Nero's Temple at El-Ashmonein archaeological site, in Minia (middle of Egypt), is considered one of the most important of all temples of Nero. This temple dates back to 1520 BC–1075 BC in the New Kingdom and was reused in the era of Nero (the Fifth Emperor of Rome). The temple construction materials are severely decayed from surrounding environmental impacts, especially contaminated water sources. The main objective of this paper is to identify the construction materials of Nero's Temple and their decay by-products. To achieve them, X-ray diffraction, micro X-ray fluorescence spectrometry, and portable Raman spectroscopy were utilized to identify the compositions and alteration by-products/degradation compounds (mainly saline efflorescence and crusts) from the construction materials, such as limestone walls, and structural mortars of the temple. In addition, a polarizing microscope was used to identify the minerals inside the construction materials and reveal the alteration of the minerals because of decay. Digital microscopy and scanning electron microscopy with EDS were used to detect decayed materials' morphological features. Finally, results showed that the main decay factor is salt attack (chlorides, sulfates, phosphates, nitrates, carbonates, and bicarbonates) for all architectural and structural elements of the temple, which have been carried to the construction materials from various sources of contaminated water (canal, sewage, and agricultural water).

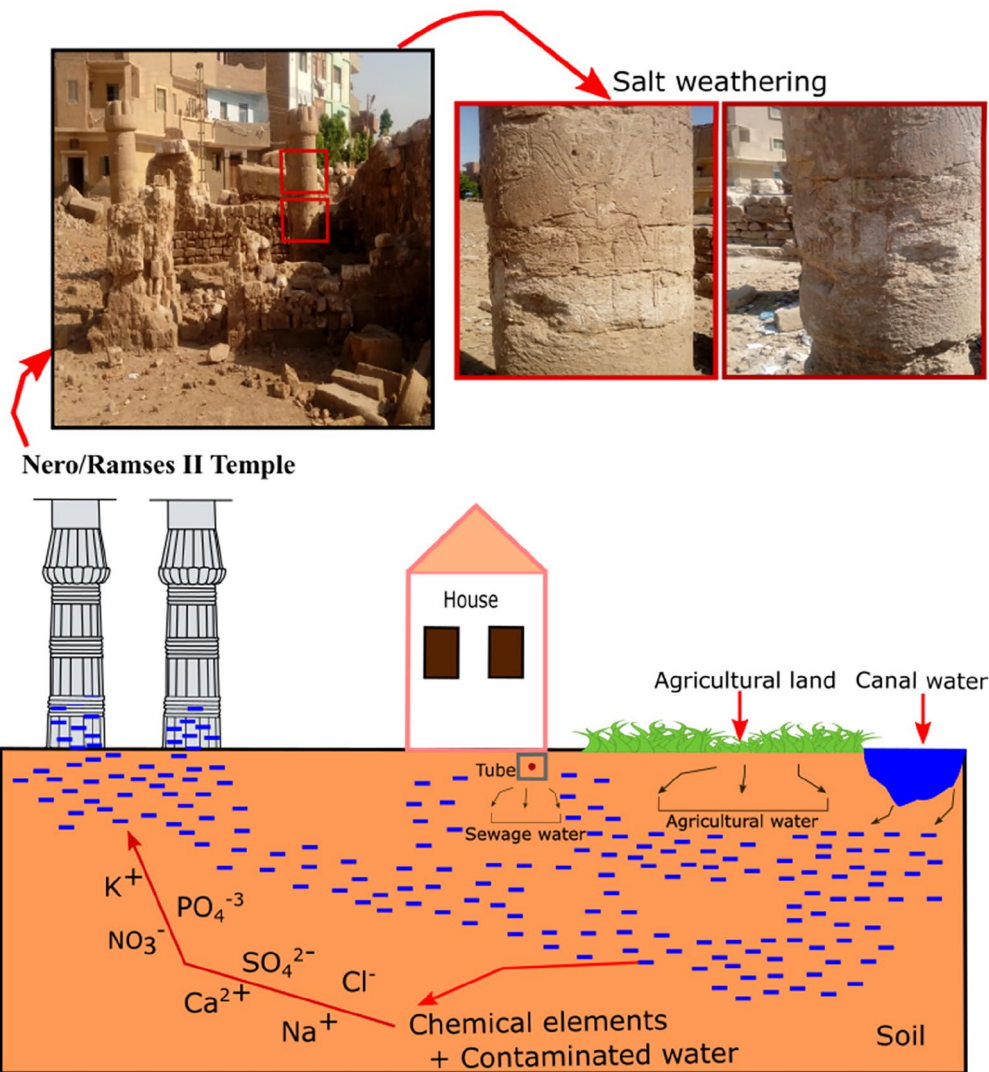
**Keywords:** Nero's Temple, El-Ashmonein archaeological site, Salt attack, Contaminated water, Building stone, Mortar, Decay, Weathering

\*Correspondence: abdelrhman.fahmy@uca.es;  
abdelrhmanmuhammedfahmy@gmail.com

<sup>1</sup> Department of Earth Sciences, Faculty of Sciences, University of Cadiz,  
Campus Rio San Pedro, 11510 Puerto Real, Spain

Full list of author information is available at the end of the article

### Graphical Abstract



### Introduction

Salt weathering can be considered one of the main problems of ancient construction materials decay in Egypt. Chlorides, nitrates, and sulfates are the most common salts that attack Egyptian stone building materials [1–3]. Many scientists specializing in geoenvironmental science, earth sciences, and heritage conservation science have made great efforts to understand and study the effects of different kinds of salt and their formation mechanisms on built heritage [4–11]. Bradley and Middleton [12] studied the soluble salt's effect on ancient Egyptian limestone due to the changes in relative humidity that decreased the durability of the stones. Tombs and ancient Egyptian monuments in Thebes were affected by salt efflorescence because of natural weathering, and human impacts [13,

14]. Aboushook et al. [15] evaluated the surrounding local environment's impact on the Egyptian stone monuments, and the quantification of the deterioration process was carried out through digital image processing. They explained that black crusts in the middle and upper parts of stone walls were formed mainly by gypsum salt and soot from vehicles and the whitish crusts in the lower parts of stone walls were formed mainly by halite. Navarro et al. [16] studied calcium and magnesium sulfate formation in situ and explained that these salts were the main decay factor of the main façade of the sixteenth-century Royal Chancery due to humidity and acidic atmosphere in the city of Granada (Spain). Erić et al. [17] said that the epsomite and hexahydrate formed as an efflorescence of limestone of Holy Virgin church walls,

and they showed that the origin of sulfate in the soil solution could be related to the presence of sulfides in the surrounding serpentinites, whose decomposition leads to the formation of sulfuric acid. They also explained that the potassium and nitrate ions required for the formation of niter most likely originate from the soil solution. Menéndez [18] studied the damage of salt and its volume variations with changing environmental conditions with a thermodynamic model (ECOS-RUNSALT). Finally, calcium sulfate or mixtures of chlorides, sulfates, and nitrates of sodium, calcium, magnesium, and potassium have been studied and estimated in salt weathering on archaeological buildings to determine the sources of degradation and their effects [19].

Hygroscopic salts have an affinity to absorb water from different sources and cause a damp rise for water to all structural elements of the building, producing severe damage [20]. Crystallization pressure is the main factor in salt weathering for heritage masonry [21]. Sodium and magnesium sulfate salts had been studied to observe their extreme effects on limestone because they are responsible for successive stone layers and crack formation and propagation inside stone samples, respectively [22–24]. Sodium chloride is considered a soluble salt with less aggressiveness for stone damage, but sodium sulfate with wet and drying cycles produces surface submicron crystals with high capillary action [25]. Lopez-Arce et al. [26] carried out an experimental study for aging on limestone samples using single magnesium sulfate and a mixture of magnesium and calcium sulfates, and sodium chloride to evaluate the damage of those salts to limestone masonry. Therefore, magnesium sulfate as a single salt increased the decay process of the stone walls of Lady of Succour Basilica in Spain with dissolution and dehydration actions (high pressure of crystallization). Then, salt crystals are forming in heterogeneous shapes inside the wall's pores, but double salts imply a lower pressure of crystallization since the double salt crystals are forming in a homogeneous shape inside the pores of the walls [27]. Fitzner [28] proposed a quantitative assessment of salt weathering carried out using monument mapping to categorize the damage into six categories: (1) no visible damage, (2) very slight damage, (3) slight damage, (4) moderate damage, (5) extreme damage and (6) very extreme damage. On the other hand, the salt susceptibility index/classification (SSI) had been used to categorize the damage resulting from salt attack as exceptionally salt-resistant, salt-resistant, salt-prone, and exceptionally salt-prone [29]. Doehne et al. [30] used an environmental scanning electron microscope to predict and assess the salt weathering of sodium chloride and sodium nitrate to monitor the grain size of the salt crystals during the crystallization process. Finally, the weathering forms of

salt attack are taffoni, honeycombs, exfoliation, flaking, blistering, scaling, micro-and macro-cracking, uniform expansion, granular disintegration (loss of compact), and delamination [31–33].

The case study (Nero/ Ramses II Temple) located at El-Ashmonein archaeological site (Minia, Egypt) is considered an example of an archaeological site affected by agricultural, urban, and subsurface water. This archaeological site is located near agricultural areas and human activities, and for this reason, some of the buildings show significant signs of deterioration due to the presence of salts. Therefore, the gathering of contaminated water in and around the construction materials of Nero's Temple is permanent. Consequently, the construction materials are currently bleeding due to severe salt weathering impacts, which led to chemical and physical alterations. For these reasons, the present paper aims to study and understand the construction materials and decay effects due to the presence of salts, and to determine the current factors that cause extreme physical and chemical decay of the architectural and structural elements of Nero's Temple. To achieve this goal, both petrographical and geochemical studies were carried out using scanning electron microscopy with EDS, digital microscopy, polarizing microscopy, X-ray diffraction, micro X-ray fluorescence spectrometry, and portable Raman spectroscopy. Finally, the salt weathering rate was categorized through alteration pattern mapping.

### Location, archaeological, and site context

Nero's Temple is located at coordinates 27°46'55"N, 30°48'11"E at El-Ashmonein archaeological site, Mellawy center, Minia Governorate. The distance between Nero's Temple and the Nile River is approximately 10.5 km, and the distance to nearby water canals (El-Ibrahimia canal and Bahr Yousef canal) is approximately 2.5 km (Fig. 1A–C). Nero's Temple is considered a small temple built on top of the ruins of the temple of Ramses II in the New Kingdom (1520–1075 BC) and decorated with many inscriptions and cartouches dating back to the period of Ramses II. Additionally, in the era of Emperor Nero, the stone blocks from the temple of Ramses II were reused in his temple construction [34, 35]. Nero's Temple was mainly constructed using the Minia limestone from the local limestone quarry with rectangular shapes. Additionally, some of these blocks were brought from different temples, such as the temple of Ramses II, where some blocks carry the name of king Ramses II. These blocks appear in the foundations and the rest of the temple [35]. The quarries in Minia were distributed from El-Bahnasa to Tell el Amarna and Mallay city and they had been utilized in different dynasties in ancient Egypt [36, 37] (Fig. 1B). For example, at Zawyet el-Amwat the limestone

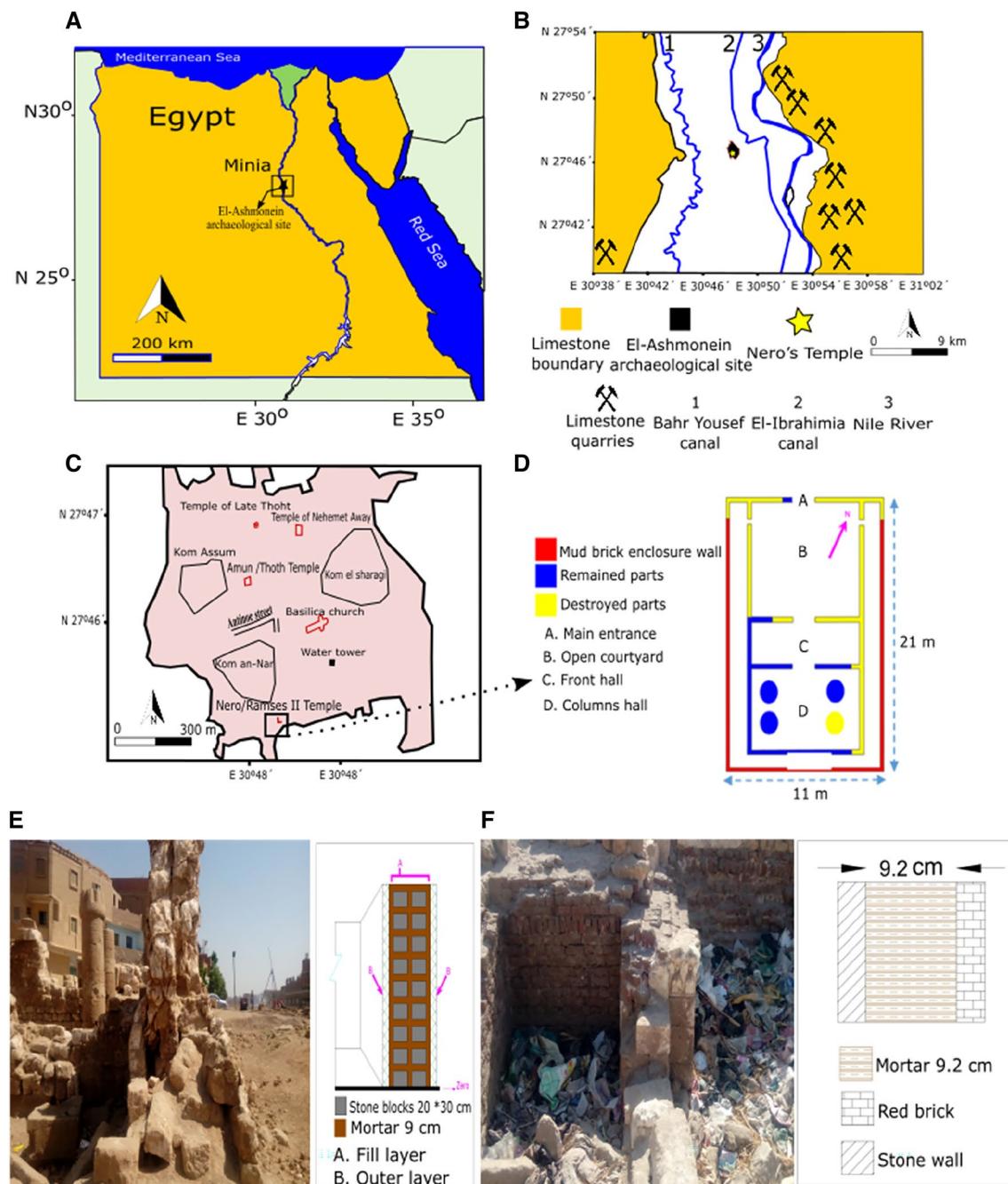


**Fig. 1** **A** General map of Egypt. Black square refers to Minia and the black star refers to El-Ashmonein archaeological site. **B** El-Ashmonein archaeological site and its location regarding the Minia limestone quarries and water sources. **C** El-Ashmonein archaeological site and its monuments; the black square refers to Nero's Temple. **D** Plan of the Nero's Temple. **E** Cross-section and the system of construction for the walls, indicating the architectural elements with dimensions of the stone blocks. **F** The cross-section for the construction materials confirms the reuse of stone blocks from Ramses II and using Roman red bricks and Roman mortar admixed together in one construction building near Nero's Temple

was prepared from this area from the New Kingdom to Roman and at Beni Hassan from the Old Kingdom to Roman [36].

Architecturally, Fig. 1D shows different architectural elements of Nero's Temple such as the main entrance of the temple in the north direction, the open courtyard, the front hall, and the columns hall in the south direction.

The main entrance of the temple located in the northern direction is damaged totally. Then, after the main gate, there is an open courtyard that is destroyed with dimensions of 8.50 m from south to north and 11 m from east to west. From the open courtyard, there is a front hall with some remaining walls with dimensions of 3.25 m from south to north and 10.20 m from east to west. Finally, the column hall has dimensions of 10.20 m from east to the west and 6 m from south to north; this hall partially exists with architectural elements such as two walls and three columns [38] (Fig. 1D). Furthermore, there is a mud-brick enclosure wall around the temple. The stone blocks were settled in horizontal and vertical systems of the wall construction, flooring, and foundations (Fig. 1E). Near Nero's Temple, there is a red brick wall from the Roman era, which confirms the reuse of stone blocks from Ramses II (Fig. 1F) [38].

The soil of the archaeological site is formed by the annual deposition of river sediments (mud and silt) during flooding events between August and October. This type of soil represents most of the territory of Minia governorate and its villages near the border of the eastern highlands and western desert, while the calcareous soil covers the land available for eastern highlands, near Maghagha and Bani Mazar cities (Fig. 2) [39]. The chemical analysis of well water used in irrigation in Minia showed that the high range of total dissolved salts varied between 1477 and 2497 mg L<sup>-1</sup> and the electrical conductivity varied between 2.24 and 3.86 dSm<sup>-1</sup>.

Additionally, after irrigation, total soluble cations ( $\text{Ca}^{2+}$ ,  $\text{Mg}^{2+}$ ,  $\text{Na}^+$ , and  $\text{K}^+$ ) and soluble anions ( $\text{Cl}^-$ ,  $\text{SO}_4^{2-}$ ,  $\text{CO}_3^{2-}$ , and  $\text{HCO}_3^-$ ) remain behind in irrigated soils as water wets out rapidly [40, 41]. Meteorologically, the average annual temperatures of the surrounding area are 36.9 °C (maximum) in June and 20.4 °C (minimum) in January. The driest months are January, February, April, May, June, July, and August. On the other hand, October is considered the wettest month with 2 mm of precipitation. January and December are the most humid months. May is the least humid month, and the average annual percentage of humidity is 38.0% [42].

## Materials and methods

### Materials

The collected samples carry six codes in Nero's Temple (NT), where NT1 (crust) was taken from a fallen highly weathered part that represents the crust. NT2 (stone) was collected from fallen parts on the ground that represents the altered stone. NT3 (crust) was taken from fallen highly weathered parts in different locations that represent the crust. NT4 (mortar) was collected from the fallen parts on the ground and represents the joint mortar of the temple. Finally, NT5 (mortar) and NT6 (mortar) were taken from the fallen parts on the ground that represent the Roman mortar. The samples were about 10 cm<sup>2</sup> and thickness of 4 cm. The samples were prepared in a solid and powdered state for analysis and examination purposes (Fig. 3A, B).

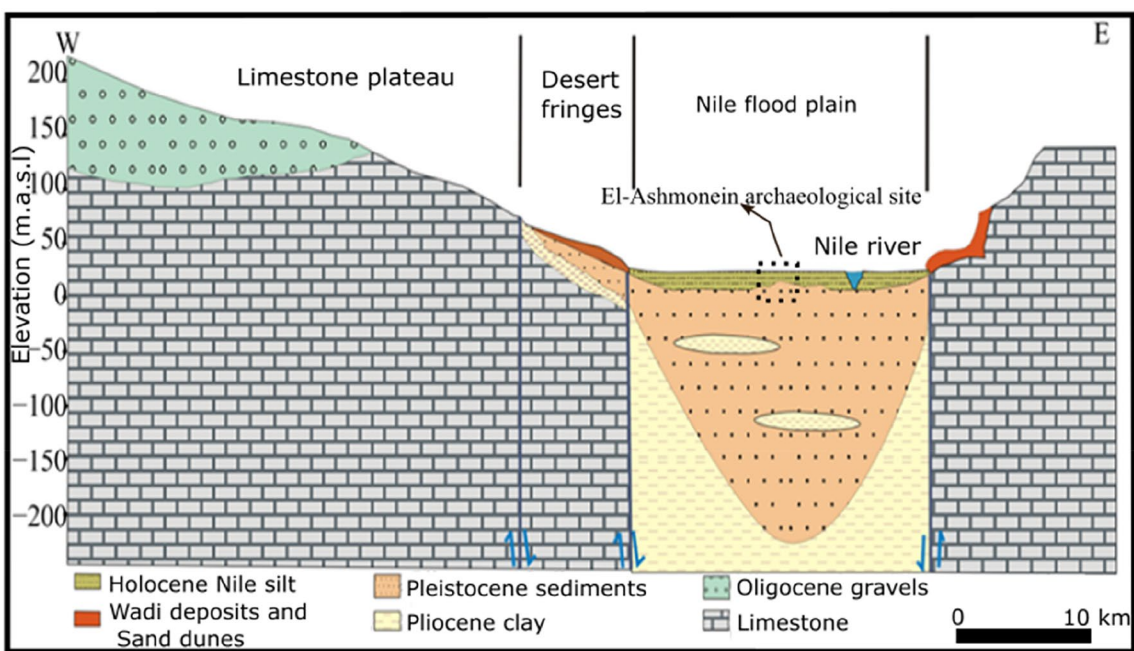
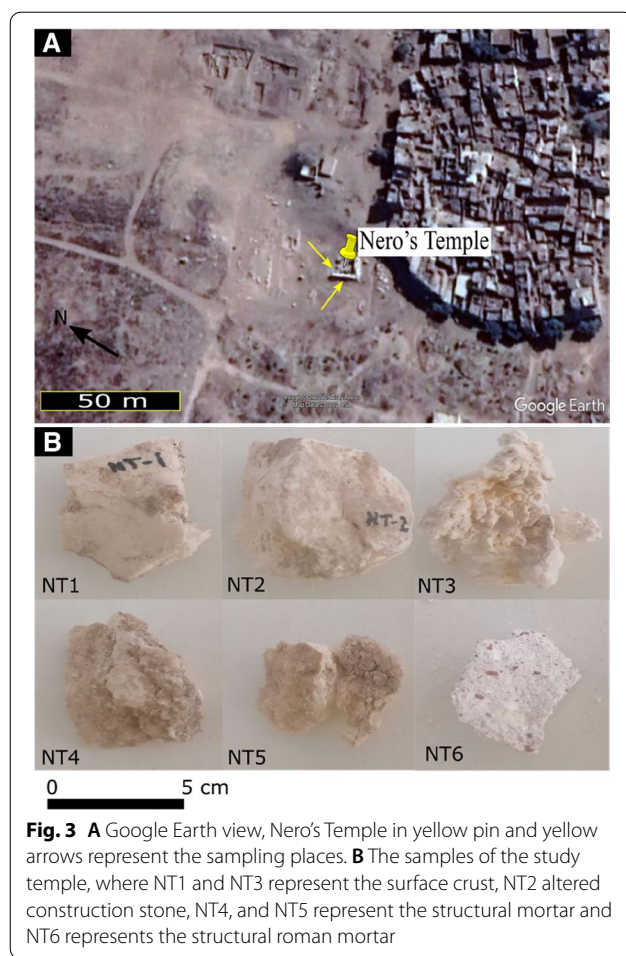


**Fig. 2** Cross-section of the geological and geohydrological features of Minia, including the study area (dotted black square refers to Al-Ashmonein archaeological site). Edited after [39]



## Methods

### In-situ and desk investigation

The in-situ investigation was performed for photographing and documentation of the current conditions of Nero's Temple during various visits to the archaeological site. A visual inspection of the temple was done to assess and record the deterioration causes and decay pathology. The surrounding environmental features were also observed to identify the sources of the contaminated water. The recording of the degradation aspects of the building materials and data collection for the architectural and structural elements for engineering drawing purposes were done using AutoCAD software 2021. Finally, salt decay identification, classification, and categorization were recorded from degradation maps.

### Analytical study

Multi-analytical and examination techniques were carried out for the qualitative and quantitative assessment of salt decay of Nero's Temple construction materials using polarizing optical microscopy (POM), X-ray diffraction

(XRD), micro X-ray fluorescence spectrometry ( $\mu$ XRF), portable Raman spectroscopy (PRS), digital microscopy (DGM), scanning electron microscopy (SEM) with EDS. These techniques let us identify the construction materials of Nero's Temple (stones + mortars) and their by-products. All these types of equipment have been hosted in the Department of Earth Sciences (UGEA-PHAM service) and Central Services of Scientific, and Technological Research (SC-ICYT) at the University of Cadiz (Spain). All the techniques described below were applied to the six selected samples.

1. Thin sections were prepared for study under an Olympus BH-2 polarizing optical microscope to identify the different minerals and altered phases of the construction materials.
2. XRD analysis was carried out to recognize the components of the samples and detect the by-products of minerals resulting from alterations and reactions between the substrate (construction materials) and geoenvironmental conditions. A Bruker D-8 Advance ECO diffractometer was used, equipped with a high-speed measurement Lynxeye detector, using the following specifications: CuK $\alpha$  radiation filtered by Ni, graphite monochromator, and fixed slots, 2theta 5° to 60° scanning angle; diffractograms were interpreted with the software EVA (Bruker-AXS).
3. Portable Raman spectroscopy (i-Raman Pro, BW TEK) BW475-532S model, equipped with a 785 nm laser, is a powerful non-destructive technique (NDT) to identify the components of the construction materials and detect the sources of the decay of the building materials of Nero's Temple.
4. A Bruker AXS M-4 Tornado sequential dispersive wave X-ray spectrometer with a Rh tube operating at 4000 W was used to identify the elemental composition of the samples and to confirm the results of X-ray diffraction.
5. A binocular microscope (USB digital microscope with stand), magnification between 20 and 400 $\times$ , and equipped with a digital camera of 1.3 Mpx was used to survey the morphological characteristics of the samples and to detect different kinds of degradation aspects.
6. A scanning electron microscope (Quanta 200), voltage between 200 V to 30 kV, resolution 3.0 nm at 30 kV and 10 nm at 3 kV, and supplied with EDAX 60 mm 2 Octane Super EDS detector was utilized for salts phases detection, degradation patterns, and elemental analysis for the detected salts.

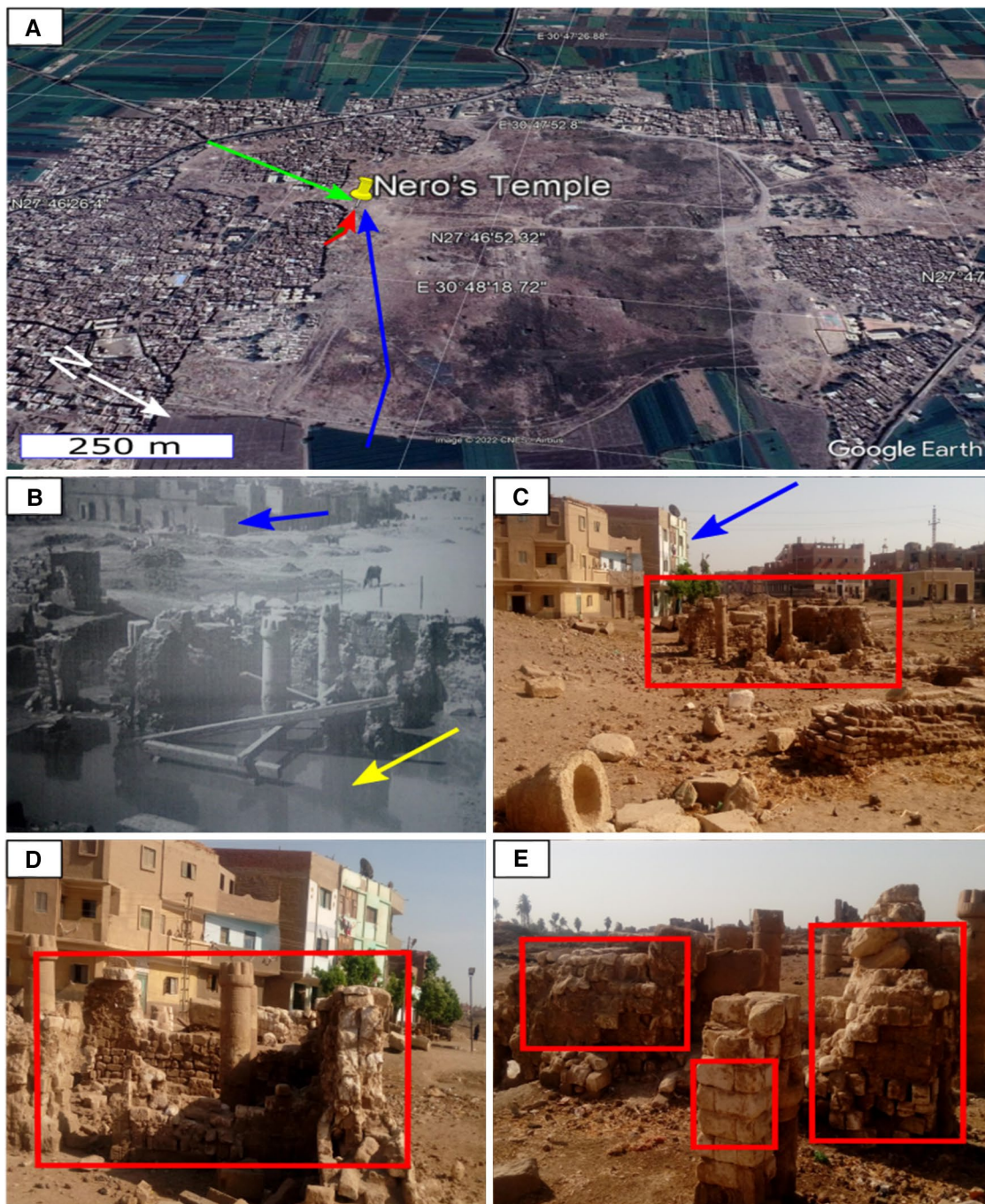


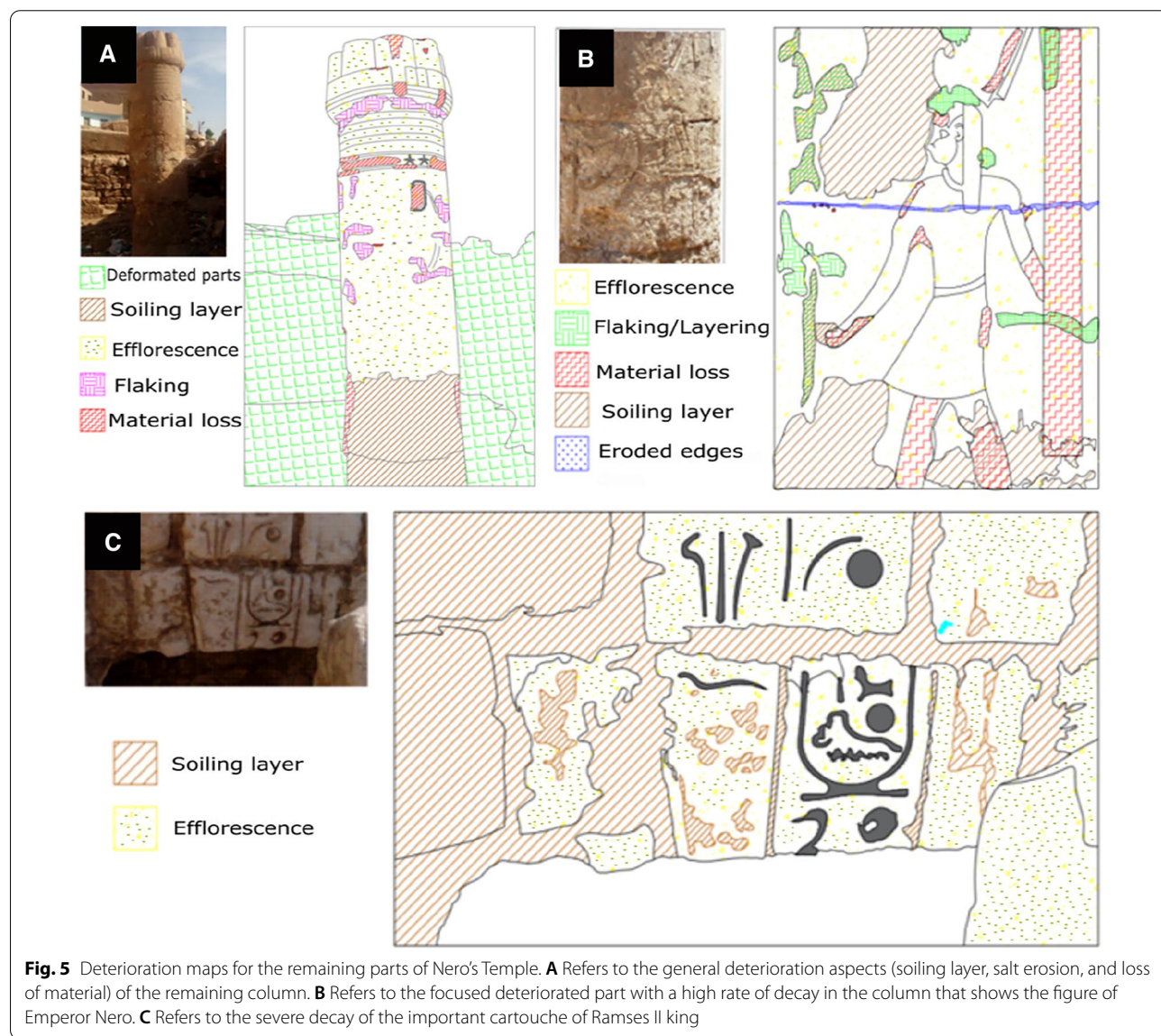
**Fig. 4** **A** Nero's Temple and the contaminated water sources. Green, red and blue arrows refer to canal water, houses, and agricultural lands, respectively. **B** The preservation state of the temple in 1983. The Blue arrow refers to the near houses and the yellow arrow indicates the gathered water, from [43]. **C–E** The current state of preservation in 2022 for Nero's Temple with its decayed and damaged elements due to salt weathering. Red rectangles refer to the degradation and deformation of the temple's architectural and structural elements. The blue arrow refers to the houses near the temple

## Results

### In-situ observation

The current preservation state of Nero's Temple is extremely decayed due to the salt erosion effects on the structural and architectural elements of the temple. From field inspections, the contaminated water from canals, agricultural lands, and sewage systems of the houses around the archaeological site, even from flooding events for several decades led to extreme chemical weathering (salt erosion) for the construction materials of the temple (Fig. 4). The distance between the temple and houses, canals, and agricultural lands are 50, 300, and 500 m, respectively (Fig. 4A). Figure 4B presents the conservation problems of the temple since 1983 due to the contaminated water around the temple. The structural

elements of the temple were in direct contact with water and the water level reached up to 1 m that affecting the durability of the construction materials. Figure 4C–E show the recent maintenance situation of the temple. It has been observed that most of the building materials have been degraded and damaged severely due to the accumulative impact of the contaminated water that resulted in high salt weathering. Moreover, the degradation maps were drawn to record the decay aspects of the structural and architectural elements (Fig. 5). It has been noticed that flaking, scaling, fracturing, efflorescence, sub-florescence, loss of material, blistering, and layering are the deterioration patterns in the construction materials of Nero's Temple due to the effect of salt weathering. In addition, soiled patinas, cracks, and microbial growth



have been also observed (Fig. 5A–C). Efflorescence and sub-florescence are the dominant decay forms in the whole stones and semi qualitatively they are estimated as about 90% of the total decay patterns in the building stones.

### Petrological study

Thin sections were prepared to investigate the composition of the archaeological samples and identify their

components, mineral alterations, and by-products because of the chemical and physical deterioration of the temple construction materials (Fig. 6). The construction material (Fig. 6 NT1 (crust) and NT2 (stone)) is a biomicritic limestone with peloids, and the appearance reflects the natural texture of the rock is well preserved. Therefore, the building material is mainly composed of calcite with rare amounts of dolomite, gypsum, quartz, halite,

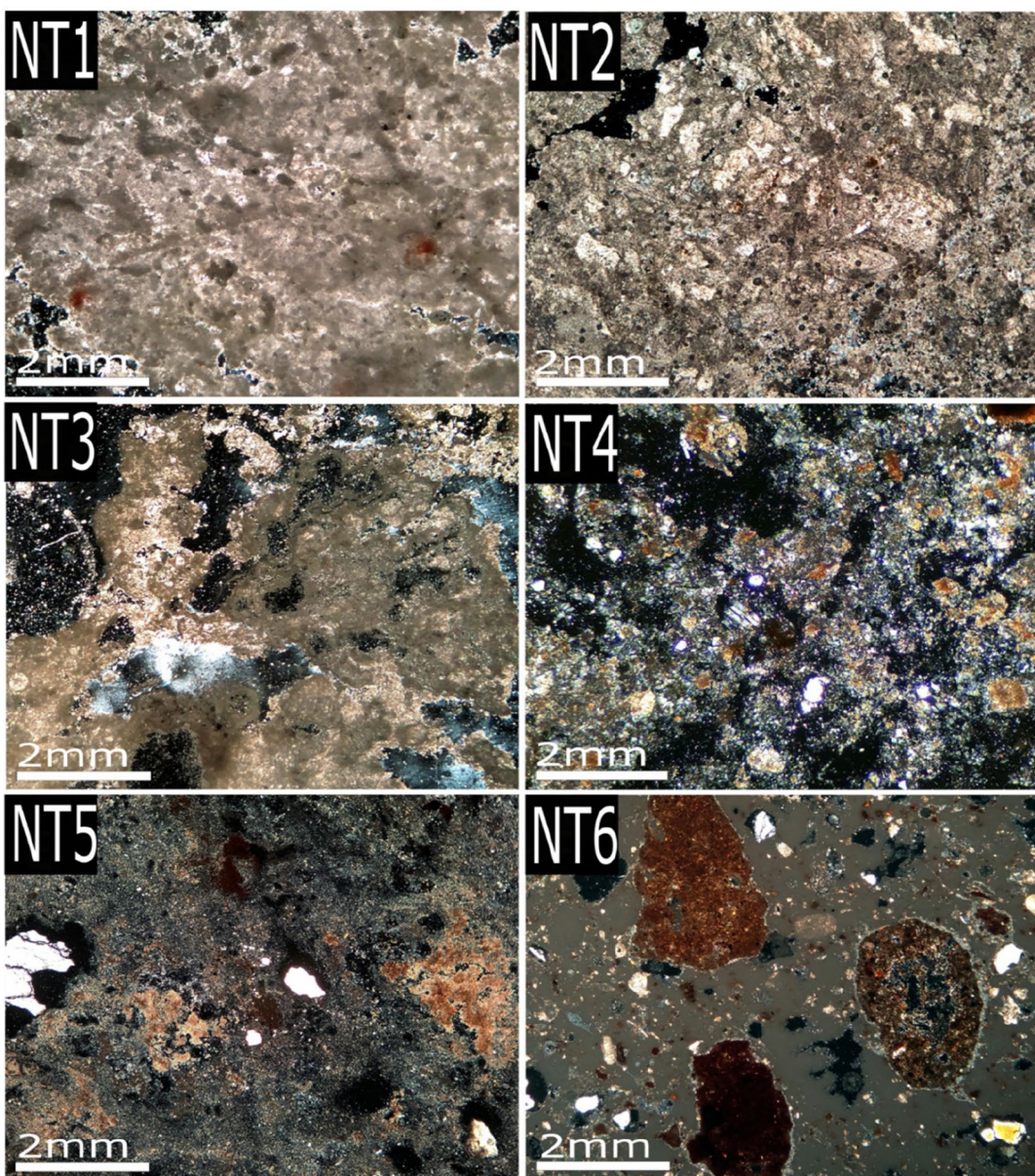


**Fig. 6** Thin section photomicrographs of limestone and mortars of Nero's Temple. (NT1, NT3) crust sections with significant amounts of pores are existed due to the dissolution and weathering processes of original carbonate minerals. (NT2) Altered biomicrite limestone as fine- to medium-grained; anhedral, sutured interlocked crystals. (NT4, NT5) Structural mortar with very fine to coarse grains and mainly composed of sand, lime, and gypsum. (NT6) Roman mortar is composed of sand with angular single grains of quartz, pottery fragments, and crushed limestone

iron oxides, and opaque minerals. Anhydrite is partially replaced by gypsum (Fig. 6 NT1).

On the other hand, NT2 is a recrystallized limestone with bioclasts such as nummulitic remains. Calcite occurs as fine- to medium-grained, anhedral, sutured interlocked crystals showing mosaic textures. Calcite is partly fragmented (granulated and crushed) and deformed into very fine-grained crystals and surrounded by the original crystals. Carbonate minerals are slightly stained and outlined by thin films of iron oxides. Additionally, some carbonate minerals are partly replaced or invaded by microcrystalline quartz or gypsum at their boundaries and interstices of grains. Dolomite occurs in rare amounts as fine-grained, subhedral to euhedral crystals in the finer matrix of the rock. Halite occurs as fine- to very fine-grained anhedral aggregates and partially fills some pore space. Moreover, NT2 shows a cataclastic effect (deformation), where coarser-grained carbonate minerals (calcite) are crushed and granulated to form a finer matrix of calcite. Pore spaces are present in significant amounts due to the dissolution of original carbonate minerals. The rock was also affected by alteration due to secondary alteration of gypsum and quartz (microcrystalline silica) replacement over carbonate. In NT 3 (crust), considerable amounts of pores are detected in the stone due to weathering.

The structural mortars (Fig. 6 NT4 and NT5) are very fine- to coarse-grained, showing porphyritic texture (coarse-grained quartz and rock fragments enclosed in a fine-grained matrix). Several irregular pores and cavities were detected in the sample. The mortar is very fine-grained to coarse and composed of rock fragments, quartz cemented by a very fine-grained matrix of carbonate (main calcite) admixed with gypsum, and minor amounts of iron oxides associated with rare amounts of halite, feldspars (plagioclase) with a lamellar appearance and biotite, muscovite, epidote, opaque minerals. Rock fragments are represented by main limestone (calcite), chert and flint and occur as coarse- to medium-grained rounded to subangular outlines and scattered in the very fine-grained sample matrix. Few microfossils are observed scattered in the rock fragment of calcite and a rare amount of clay (Fig. 6 NT4 and NT5). Quartz and feldspars occur as medium- to fine-grained surrounded to subangular outlines and cemented by a mixture of a very fine-grained matrix. Iron oxides and opaque minerals occur as fine- to medium-grained scattered in the sample. Halite is represented by traces enclosed in some pore spaces. Mafic minerals are fine-grained and observed in the matrix of the sample. A significant number of irregular pores with different shapes and sizes are scattered in the sample. Figure 6 NT6 represents different

kind of mortar (Roman mortar used in the period of Emperor Nero) mainly composed of pottery fragments, sand (quartz) and lime (calcite), and single grains of quartz are clearly observed.

The essential components for mortars (Fig. 6 NT4, NT5, and NT6) are affected by deformations, showing microcracks in quartz, rock fragments, and corroded boundaries and edges. Several pore spaces and cavities (vugs) are present due to the alteration and dissolution of the essential components such as calcite and calcium sulfates. Biotite and mafic minerals are partly to highly affected by alteration.

## Mineralogical and elemental analysis of the construction materials

### Mineralogical analysis

X-ray diffraction was used to identify the mineral composition of the construction building materials and the structural mortar semi-quantitatively (Table 1). Salts and the alteration by-products on the surfaces of the stones were analyzed. Sixteen minerals were detected that were composed of mainly hydrated and anhydrous sulfates, nitrates, carbonate, phosphates, and chlorides. For crusts (Table 1 NT1), calcite is the main constituent. In addition to the degradation compounds, they are classified as chlorides (halite and sylvite) and bicarbonates (nahcolite,  $\text{NaHCO}_3$ ). Calcite and halite existed as very abundant, while nahcolite and sylvite existed as scarce. In Table 1. NT3, calcite was detected as a common mineral. Degradation compounds were detected and classified as chloride (halite), nitrate (humberstonite,  $\text{Na}_7\text{K}_3\text{Mg}_2(\text{SO}_4)_6(\text{NO}_3)_2 \cdot 6\text{H}_2\text{O}$ , and ungemachite,  $\text{K}_3\text{Na}_8\text{Fe}(\text{SO}_4)_6(\text{NO}_3)_2 \cdot 6\text{H}_2\text{O}$ ), and anhydrous sulfate (anhydrite). Halite appeared as very abundant, calcite and humberstonite appeared as abundant, and ungemachite and anhydrite appeared as scarce. For stone blocks (core) (Table 1 NT2), calcite was detected as the main constituent of stone blocks, while halite was detected as an abundant alteration compound.

For structural mortar (Table 1 NT4), calcite, quartz, and gypsum are the main constituents, which were composed mainly of lime, gypsum, and sand. Additionally, the alteration by-products were detected and classified as hydrated sulfate minerals (gypsum, bassanite, and starkeyite ( $\text{MgCaSO}_4 \cdot 4\text{H}_2\text{O}$ )), anhydrous sulfate (anhydrite), chloride (halite), phosphates (brushite), carbonates (natron), and silicates (illite)). Halite appeared very abundant, and the rest of the compounds appeared as scarce. On the other hand, in Table 1 (NT5) calcite, quartz, and gypsum are the main constituents of the mortar, which was also composed mainly of lime, gypsum, and sand. Additionally, the alteration by-products were detected

**Table 1** Semi-quantitative mineralogical analysis of the samples, where NT1 and NT3 represent the surface crust, NT2 altered construction stone, NT4, and NT5 represent the structural mortar and NT6 represents the structural roman mortar

	NT1 Crust	NT2 Stone	NT3 Crust	NT4 Mortar	NT5 Mortar	NT6 Mortar
Cal	+++	+++	++	+	+	+
Hl	+++	++	+++	+++	+	
It				+		
Hbe			++			
Ugm			+			
Gp				+	++	
Anh			+	+	+	+
Bas				+		+
Brt				+		
Qz				+	+	+
Na				+		
Mc						+
Sep						+
Nah	+					
Stk				+		
Stg						+
Syl	+					+

Cal calcite, Hl halite, It illite, Hbe humberstonite, Ugm ungemachite, Gp gypsum, Anh anhydrite, Bas bassanite, Brt brushite, Qz quartz, Na natron, Mc microcline, Sep sepiolite, Nah nahcolite, Stk starkeyite, Stg strengite, Syl sylvite, x scarce, xx abundant, xxx very abundant. Minerals symbols after [44] except for It illite, Hbe humberstonite, Bas bassanite, Brt brushite, Na natron, Nah nahcolite, Stk starkeyite, Stg strengite, Syl sylvite

and classified as anhydrous sulfate (anhydrite) and chloride (halite). Gypsum appeared abundant, and the rest of the compounds appeared as scarce.

Structural Roman mortar (Table 1 NT6) is composed of calcite, quartz, microcline, and sepiolite. As compounds of degradation, hydrated sulfate (gypsum and basanite), anhydrous sulfate (anhydrite), and phosphates (strengite  $\text{FePO}_4 \cdot 2\text{H}_2\text{O}$ ) were detected. Calcite is present as very abundant, and the rest of the compounds are present as scarce.

Furthermore, the samples were analyzed using Raman spectroscopy with an extended wavelength range from 100 to 2000  $\text{cm}^{-1}$ . The results of the analysis responded well to XRD results. The majority of the minerals and salts detected by XRD were found in the Raman analysis such as calcite, quartz, halite, gypsum, anhydrite and brushite. Calcite is a common mineral in all samples and is identified at 156, 284, 711, and 1086  $\text{cm}^{-1}$  (Fig. 7). In this regard, [45] confirmed that the carbonate minerals show four prominent absorption bands in the regions 890–870, 720–700, 1000–1100, and 1450–1420  $\text{cm}^{-1}$ , and calcite and dolomite groups are characterized by the presence of peaks at 288 and 309  $\text{cm}^{-1}$ . The anhydrite phase, which is completely altered from gypsum, is identified at 417, 500, 611, 629, 676, 1018, 1130, 1160, 1582, and 1610  $\text{cm}^{-1}$  (Fig. 7). Salt of brushite signed at 1000  $\text{cm}^{-1}$ . Finally, halite as common salt in all samples is

identified between 100 and 430  $\text{cm}^{-1}$ , as shown in NT2, NT4, and NT6 (Fig. 7).

#### Elemental analysis

Micro X-ray fluorescence was carried out to identify the elements for each sample of construction materials and to confirm the results of X-ray diffraction (Table 2). The results responded well to the mineralogical analysis results, where the analysis showed the existence of salt ions ( $\text{Ca}^{2+}$ ,  $\text{Mg}^{2+}$ ,  $\text{K}^+$ ,  $\text{Na}^+$ ,  $\text{Al}^{3+}$ ,  $\text{SO}_4^{2-}$ ,  $\text{NO}_3^-$ , and  $\text{Cl}^-$ ), and the most dominant ions were sulfate, chloride, sodium, and calcium. Chloride, sodium, and sulfate ions were significant in NT1, NT2, NT3, and NT4. In NT5 and NT6, the most predominant ions were silicate, chloride, and sulfate. Magnesium appeared significantly in NT3. Iron and aluminium ions appeared clearly in NT5 and NT6.

#### Microscopic investigation

##### Digital microscope

Textural aspects from digital microscopy were made to examine and investigate the decay and salt weathering of the Nero temple building materials, such as limestone, crusts, and mortars (Fig. 8). Efflorescence and sub-florescence exist in the building materials because of salt weathering, where there is a loose salt deposit

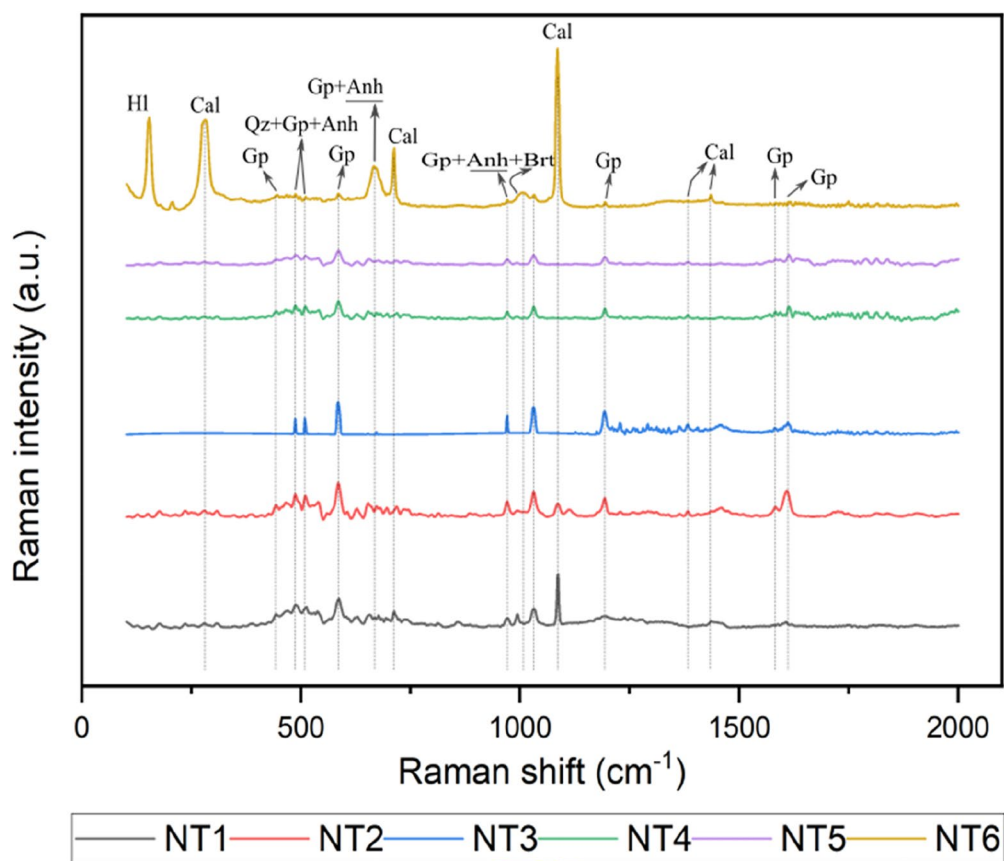


**Fig. 7** Raman spectra for NT1 and NT3 (Crust) NT2 (altered stone), NT4 and NT5 (structural mortar), and NT6 (structural roman mortar). Anh (anhydrite); HI (halite); Cal (Calcite); Gp (gypsum); Brt (brushite); Qz (quartz). Minerals symbols after [44] except for Brt (brushite)

**Table 2** Chemical composition of the six construction materials

	NT1 Crust	NT2 Stone	NT3 Crust	NT4 Mortar	NT5 Mortar	NT6 Mortar
CuO	0.003	–	0.007	–	0.002	–
Al <sub>2</sub> O <sub>3</sub>	0.795	–	0.725	0.662	1.009	4.039
SiO <sub>2</sub>	1.957	0.250	2.134	8.100	12.174	40.458
K <sub>2</sub> O	8.629	2.809	17.833	3.073	1.908	0.589
CaO	26.059	37.729	11.768	29.403	44.942	49.997
Cl	16.506	13.374	7.111	8.419	1.246	–
TiO <sub>2</sub>	0.046	–	0.086	0.119	0.342	0.528
Fe <sub>2</sub> O <sub>3</sub>	0.185	0.015	0.422	0.509	1.042	2.914
MgO	1.615	0.291	3.853	1.680	1.187	0.298
SO <sub>3</sub>	15.259	6.509	30.738	32.255	33.755	0.625
Na <sub>2</sub> O	28.903	39.000	25.241	15.546	2.130	0.625
ZrO	0.008	0.004	0.012	0.012	0.021	0.025
Cr <sub>2</sub> O <sub>3</sub>	0.033	0.009	0.010	–	0.010	–
SrO	–	0.009	0.002	0.048	0.212	0.021
P <sub>2</sub> O <sub>5</sub>	–	–	0.052	0.150	–	0.461
MnO	–	–	0.005	0.012	0.016	0.044
V <sub>2</sub> O <sub>5</sub>	–	–	–	0.009	–	–

Major and minor elements are expressed in wt % oxides

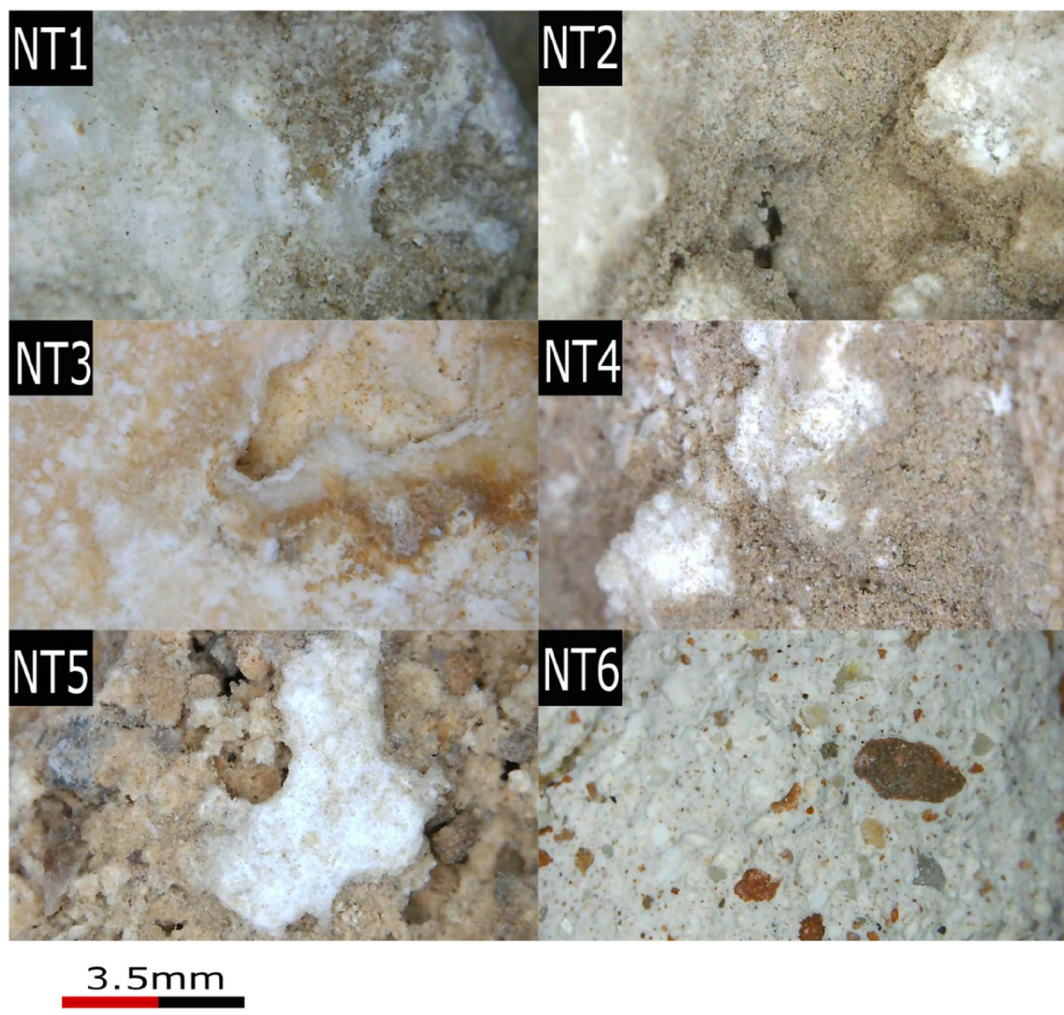


**Fig. 8** Microphotographs for the construction elements to detect the texture features of decayed stones and mortars. NT1 (crust), NT2 (altered stone), NT3 (crust), NT4 (mortar), NT5 (mortar) and NT6 (mortar). Salts precipitation and disintegration are dominant decay patterns for all samples

on the surface mixed with the soiling layer and a loose salt deposit below the surface of the construction materials, as well as pores, layering, and disaggregation are observed (Fig. 8 NT1 and NT2). In Fig. 8 NT3, the morphological feature indicates the disintegrated texture of the stone. The precipitation of the salt is observed and the flaking decay pattern of the stone surface is detected due to the salt erosion. In Fig. 8 NT4, micro-fissures, soiling, and surface crust are noticed as degradation patterns for the structural mortar. Salt precipitation on the surface is seen as well. In Fig. 8 NT5, the surface texture shows an extreme disintegration for the structural mortar with many pores. Efflorescence and sub-efflorescence are observed on and below the surface. Figure 8 NT6 presents the textural properties of the Roman Mortar. The various grain sizes of the quartz and Calcite fragments

are observed. Moreover, calcite is found as a matrix, and pottery fragments are observed as well. Pores and salt deposits are detected. Finally, pores are seen on the surface and below the surface of the construction materials as intrinsic component and their size can be increased due to dissolution processes for the stone minerals because of water existing and its fluctuations. Salt erosion is considered the most dominant degradation pattern in all samples.

#### **Scanning electron microscope investigation (SEM)-EDS**

The microstructural and morphological features reflected the severe decay conditions of the construction elements; the disintegration and salt weathering were clear and detected. Halite was detected as the most dominant salt in cubic shapes and existed in euhedral, subhedral, and

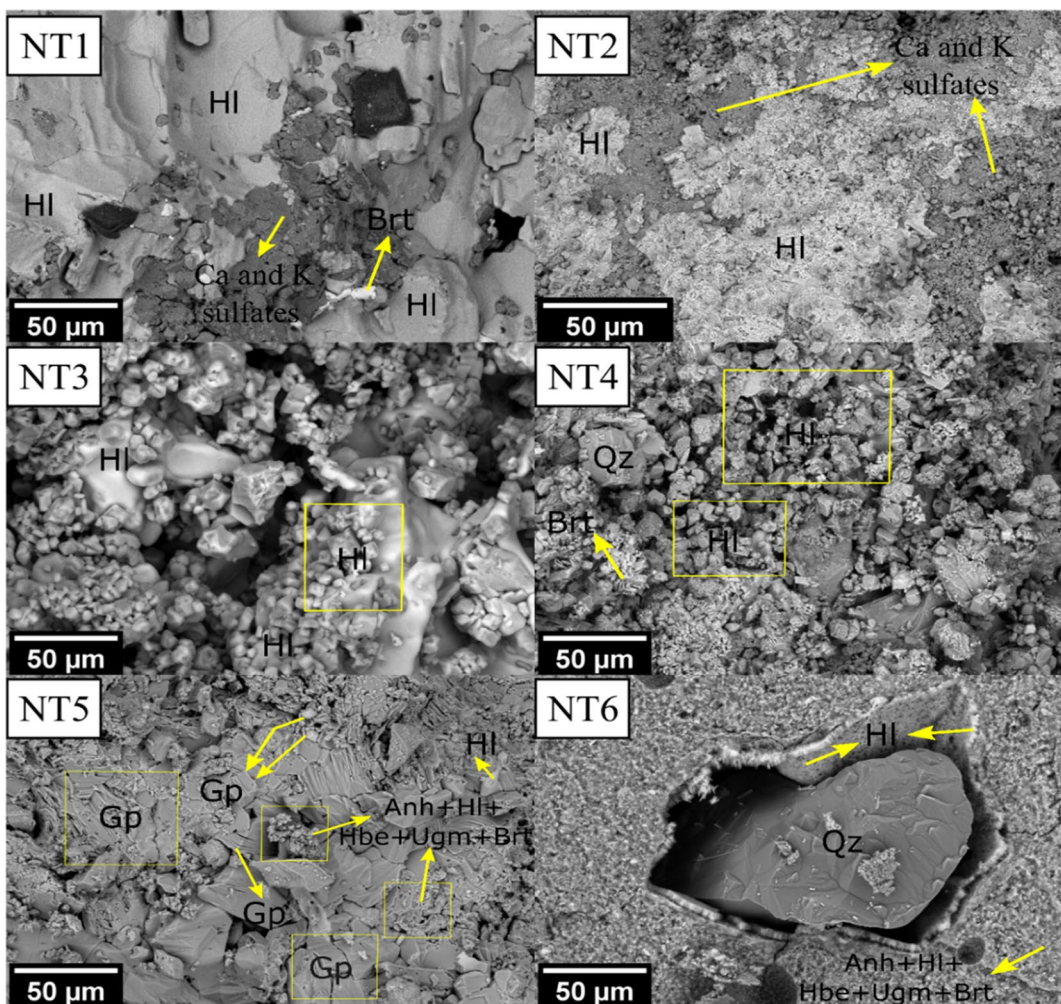


**Fig. 9** General morphological view of the six samples (NT1-NT6). In NT1 to NT4, the halite (light gray) and Ca and K sulfates (dark grey) crusts are shown, with some calcium-phosphate crystals (in white) and black organic particles. NT5 shows a crust composed mainly of layered and mesostructured gypsum with traces of Na and Cl (halite) and sulfates. In NT6, there is a pore with a quartz grain with signs of corrosion and a film with acicular-planar halite crystals, and a matrix composed of calcite and a mixture of calcium silicates, halite, sulfates, and calcium-phosphate. HI (halite); Gp (gypsum); Anh (anhydrite); Brt (brushite); Qz (quartz); Hbe (humberstonite); Ugm (ungemachite). Minerals symbols after [44] except for Brt (brushite)

anhedral forms, as halite crystals are unstable due to their high solubility. Halite is present in the liquid phase and integrated with the crystallized crystals in all samples. This halite has a massive texture and covered the grains, as well as interacts with the stone surfaces, as shown in NT1, NT2, NT3, NT4, and NT5 (Fig. 9). Gypsum existed in layers, nodules, and flower shapes between and around the grains, and gypsum crystals were thin and looked like needles with smooth surfaces, as shown in NT4 and NT5 (Fig. 9). Bassanite was detected in different shapes between square rods and massive shapes, as shown in NT4 and NT6 (Fig. 9). Moreover, anhydrite was detected in euhedral shapes and massive amounts in clear

nodule shapes, as shown in NT3, NT5, and NT6 (Fig. 9). In NT3 (Fig. 9), double salt crystals of humberstonite and ungemachite exist in isometric shapes and integrate with other sulfate salts and halite. Finally, microcracks and cavities were detected in the mortar and stone blocks, which reflect the chemical and physical weathering of the construction materials.

Elemental analysis (EDS) was carried out to prove the existence of different kinds of salts (sulfates, chlorides, phosphates, nitrates, carbonates, and bicarbonates) that caused high salt decay for the temple construction materials. The EDS results responded well to the XRD, Raman analysis, and  $\mu$ XRF results. Sodium, chlorine, calcium,

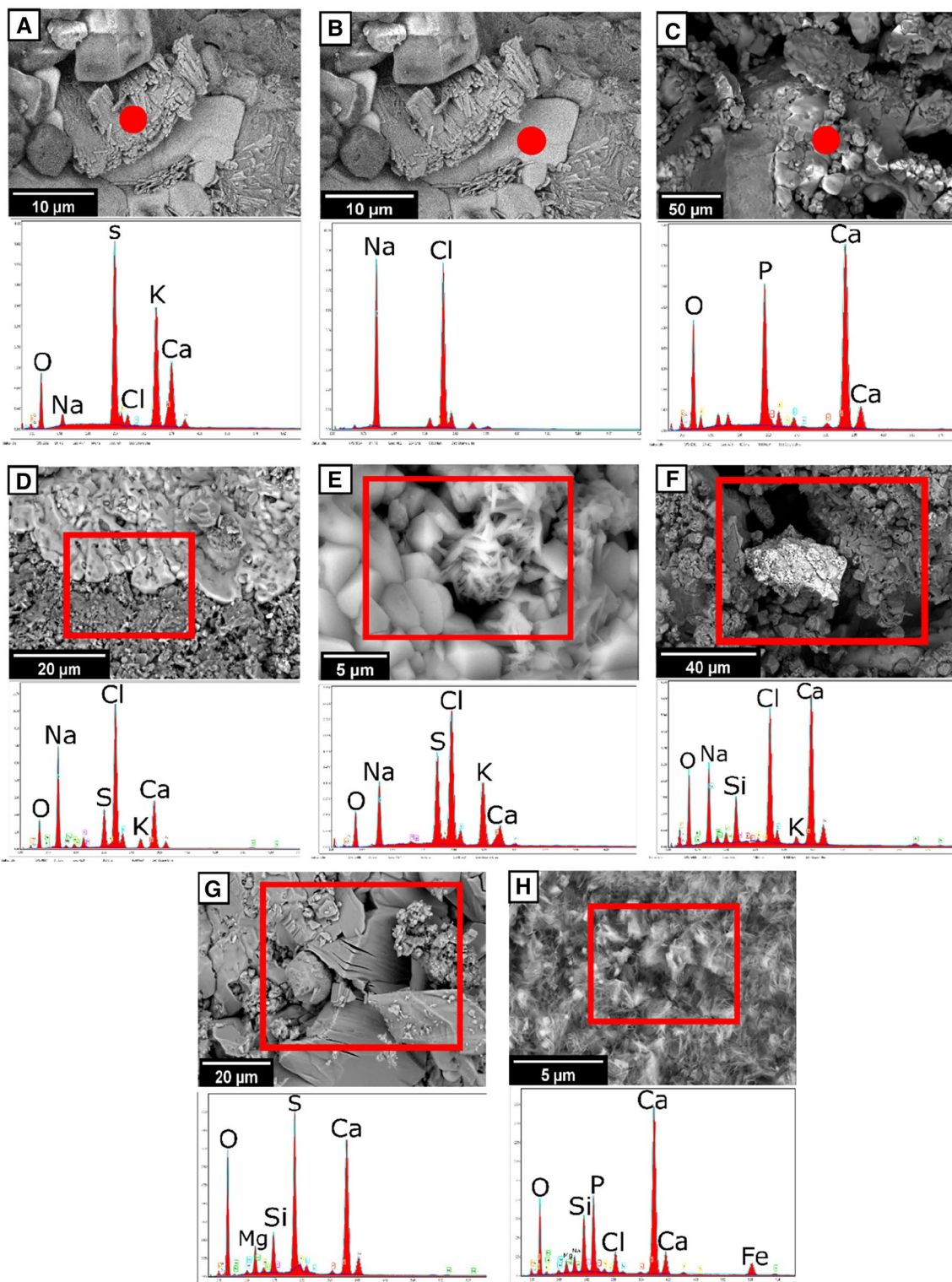


**Fig. 10** EDS results of detailed points and areas (dots and rectangles areas, respectively) for the temple construction materials. In sample NT1, **A** refers to sulfates, **B** refers to chlorides, and **C** refers to phosphates. In NT2 (**D**) and NT3 (**E**), the red rectangles refer to two types of salt attack (sulfates and chlorides). In NT4 (**F**), quartz grains of the mortar surrounded by halite can be distinguished. NT5 (**G**) shows an example of a salt attack of sulfates of structural mortar and NT6 (**H**) shows a different kind of salt attack (phosphates and chlorides) over the Roman mortar

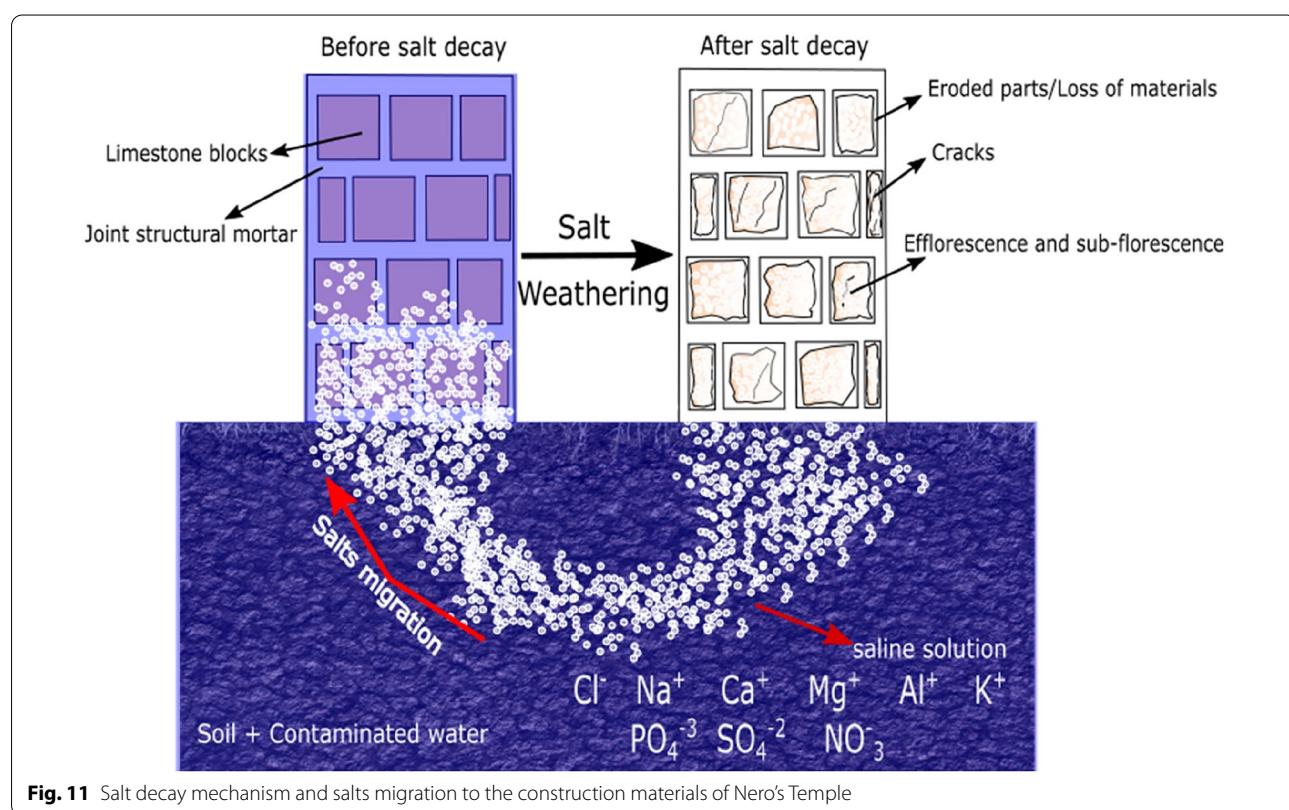
sulfur, magnesium, phosphorous, and potassium were detected as the most common ions. Chlorine and sodium were the dominant elements in all samples, as shown in NT1, NT2, NT3, NT4, and NT6 (Fig. 10). Phosphorous was detected clearly in samples NT1 and NT6, as it is shown in Fig. 10 (NT1-A and NT6-H) confirming the presence of phosphate salts.

## Discussion

Results revealed that limestone (biomicritic) is the main building material of Nero's Temple, which was quarried from Minia formations. Significant lime gypsum mortar appeared in the results and was confirmed by the polarizing microscope, micro X-ray fluorescence, Raman spectroscopy, and scanning electron microscope with EDS for the samples (NT 4 and NT 5). This mortar consists of lime, gypsum, and sand, dating back to the Ramses II era (Egyptian New kingdom 1540–1075 BC). In this regard, gypsum was used in the horizontal and vertical structural joints of construction materials. Gypsum was added to the lime to have a mixture of so-called gypsum concretes, and this technology was also found in tell Amarana in Minia [46]. Roman hydraulic lime mortar from the era of Emperor Nero (50–54 CE) was detected in NT 6, which consists of lime, quartz, pottery fragments, and clay additions. Pottery fragments, microcline and sepiolite

(pozzolans) were detected by analytical techniques as a source of silica and alumina in the mortar combination to strengthen the hydraulicity of the mortar. Accordingly, Caro [47] confirmed that Romans added ceramics to the lime mortars to improve their durability and hydraulicity properties.

These previous construction materials have been subjected to the accumulated impact of salt weathering. In this sense, chlorides, hydrated Ca-Mg-Na-Al-K sulfates, nitrates, phosphates, carbonates, and bicarbonates were detected as precipitated salts. From the site investigation, different sources of water (canals, sewage, and agricultural) near the temple are the clearest proposals as sources of the decay salts. In this sense, the mechanism of salt weathering for the temple was due to the rising up of the contaminated water from the soil solution under the temple by capillary action/suction through the fine pores. Then, the capillaries draw water from the soil beneath the temple to the whole building structures against the force of gravity, leading first to the damp, which carries up the salts to the base of the temple walls, and then to the whole masonry materials. When the water evaporates from the walls, the salts are left behind. Repeated wetting and drying cycles with daily and seasonal changes led to the cyclic precipitation of salts and resulted in severe salt attacks on the structural and architectural elements



of the temple (Fig. 11). In this regard, Young [48] confirmed this mechanism of salt attack and explained that the quality of the building materials and of construction and subsequent maintenance, climate, and soil conditions are strong drivers of the severity of salt-damp problems. Moreover, Abdel-Mageed et al. [40] confirmed that the water source used for irrigation in Minia contains sodium, chlorides, and calcium and magnesium ions, and they indicated a high concentration of total soluble salts (TSS) (ranging from 1477 to 2497 mg L<sup>-1</sup>), chloride and bicarbonate concentrations, with a water electrical conductivity ranging from 2.24 to 3.86 dS m<sup>-1</sup>.

Halite (NaCl) is present in all analyzed samples as abundant to very abundant, and sylvite (KCl) is only present in NT1 as scarce (crusts). Halite is considered the main decay anhydrous salt for construction materials and structural mortars. In this sense, Derluyn et al. [49] explained that halite plays a serious role in the salt crystallization decay of the construction elements because it can dissolve in water or in humid environments and precipitates as cubic crystals, but the solubility of sodium chloride is only slightly temperature-dependent. The precipitation of halite crystals accumulates on the stone surfaces and causes efflorescence (on the surface) and sub-efflorescence (beneath the surface). After forming halite crystals on the surfaces, the crystals with drying cycles lose the water and cause blistering, layering, micro-cracking, granular disintegration, flaking, horizontal cracking, and scaling for building stones. Furthermore, chloride and sodium ions in the irrigation and contaminated water react with limestone (carbonates) as the main building material to produce a soluble salt called calcium chloride and other soluble salts such as sodium carbonate, calcium chloride, and sodium carbonate. These phases react with each other to produce calcium carbonate (insoluble salt) and sodium chloride (soluble salt) as a crust. Consequently, many cycles of dissolution and crystallization led to weakness and decreased the strength and bearing capacity of the temple construction materials.

Gypsum ( $\text{CaSO}_4 \cdot 2\text{H}_2\text{O}$ ), bassanite ( $2\text{CaSO}_4 \cdot \text{H}_2\text{O}$ ), and anhydrite ( $\text{CaSO}_4$ ) were detected in some samples as alteration by-products in NT1, NT4, NT5, and NT6, but in NT4 and NT5, gypsum existed as a secondary adding to the lime gypsum mortar. The construction materials deteriorated by gypsum, and it transformed into the bassanite phase (most likely by dissolution–precipitation, starting from the surface in contact with the fluid or humidity). This phase represents a secondary stage, as it is unstable with respect to anhydrite. Additionally, Vaniman et al. [50] mentioned that the situation might also be complicated by groundwater dynamics, wherein static batch systems only gypsum precipitates, but in flowing systems, gypsum plus anhydrite precipitates.

Cation exchange reactions can occur between clay minerals and Mg-sulfates in the absence of free liquid ( $\text{H}_2\text{O}$ ), accompanied by the formation of gypsum or bassanite. The dehydration and hydration processes of gypsum are considered a critical point in stone decay, as when dehydration occurs, the stone surfaces are converted to powder form and lose their cohesiveness. The dehydration of gypsum occurs at temperatures above 42 °C or where highly saline water exists and the temperature at the archaeological site of Nero's Temple could reach 44 °C, especially in the summer months. For this, Vaniman et al. [50] confirmed that in diluted solution, anhydrite forms at somewhat generally above ~40 to 60 °C. However, the activity of water has a significant effect, and in concentrated solutions, anhydrite can form at temperatures as low as 18 °C, with a water activity of 0.75. Gypsum exists as white surface crusts that are common in arid environments and produces silt-sized crystals several centimeters in length. Anhydrite exists as an alteration mineral and reflects the severe bleeding of the stone blocks, where it is existed as abundant to very abundant in most of the temple samples.

Hydrated magnesium sulfate (starkeyite,  $\text{MgSO}_4 \cdot 4\text{H}_2\text{O}$ ) was detected in the NT4 sample (Mortar). In this context, Balboni et al. [51] explained that the hydration and dehydration of magnesium sulfate salts ( $\text{MgSO}_4 + \text{H}_2\text{O}$ ) in many examples were due to their presence in contaminated water sources and they can cause damage in the drying and during condensation or uptake of rain and groundwater. Additionally, Gázquez et al. [52] confirmed that the precipitation of hydrated Mg sulfates plays a severe role in the decay rate of the architectural elements of buildings.

On the other hand, humbertonite ( $(\text{Na}_7\text{K}_3\text{Mg}_2(\text{SO}_4)_6(\text{NO}_3)_2 \cdot 6\text{H}_2\text{O}$ ) was detected as abundant salt and ungematchite ( $(\text{K}_3\text{Na}_8\text{Fe}(\text{SO}_4)_6(\text{NO}_3)_2 \cdot 6\text{H}_2\text{O}$ ) was detected as scarce salt in the NT3 sample (crust). These salts are considered composite because they are composed of sodium, calcium, magnesium, iron sulfate, and nitrate ions together. Benavente et al. [27] confirmed that pigeon droppings lead to crust formation and deposits, and their lixiviated water produces efflorescence, therefore these kinds of salts could be present due to the continuous pigeon droppings. Balboni et al. [51] also reported that sodium sulfate causes slower damage during the rewetting process than magnesium sulfate and depends on the viscosity of the solution. However, it could cause extreme damage to the building materials, as it expands over 300% concerning another mineral conversion, especially from anhydrite [53]. Rodriguez-Navarro et al. [54] concluded that sodium sulfate is damaging mainly because it undergoes a high degree of volume change when hydrated. Moreover, nitrate salts accumulate anywhere where nitrogen compounds and Na, K, Mg, and Fe ions exist

[55]. The source of nitrogen and Na, K, Mg, and Fe in the present study is from the soil solution around Nero's Temple. In this sense, Eric et al. [17] confirmed as an example that the potassium and nitrate ions required for the formation of nitrogen most likely originate from the soil solution.

Alkali-bicarbonate and carbonate salts (nahcolite,  $\text{NaHCO}_3$ , and natron,  $\text{Na}_2\text{CO}_3 \cdot 10 \text{ H}_2\text{O}$ ) exist in the samples of NT1 (crust) and NT4 (mortar), respectively. Their presence was probably due to the condensation process and saline soil solution, and these alkali sodium carbonate salts could contribute to salt efflorescence, layering, cracking, and blistering for the building materials. In this sense, [56, 57] confirmed that efflorescence is mainly composed of alkali sodium salts due to rising dampness and the possible accumulation of water from flood events and saline soil.

Additionally, brushite ( $\text{CaHPO}_4 \cdot 2\text{H}_2\text{O}$ ) and strengite ( $\text{FePO}_4 \cdot 2\text{H}_2\text{O}$ ), as phosphate minerals, were found as scarce in samples NT4 (mortar) and NT6 (mortar). The deposition of phosphates could be associated with the presence of fresh or desiccated bats/birds [58, 59]. Besides phosphates may come from irrigation water and wastewaters. Brushite and strengite salt affected the durability of Nero's Temple during the rising up of water from the ground to the structural elements of the temple. Water carries phosphate ( $\text{PO}_4^{3-}$ ) ions, which are released from irrigation water or wastewaters to react with the calcium ( $\text{Ca}^{2+}$ ) ions of limestone in building materials.

The various mentioned salts could cause a high mechanical salt load for the building materials, as each salt has its own pressure parameter during crystallization, hydration, dehydration, hygroscopic expansion, thermal expansion, and capillary [60]. For example, Fernandez [61] said that magnesium and sodium sulfate salts have the ability to absorb water into their structure, which changes the lattice parameters to form a new crystal. The addition of water to crystallization often causes an increase in the molar volume of the salt and a change in the crystal structure, and this process is called hydration pressure. Accordingly, in the present study, the dehydration of gypsum into bassanite and anhydrite could be accompanied by thermal expansion pressure during the dehydration process [62]. In addition, anhydrous and hydrated sulfates exist, and according to Stambolov and Van Asperen De Boer [63] anhydrous sulfates are precipitated in the pores from their oversaturated solutions as hydrates, and as the evaporation of water proceeds, the deposits of these hydrates drain out. The anhydrous salts formed are thus microcrystalline aggregates due to their fine porous structure. They promote the flow of more solutions from the interior of the pore to the surface. An increase in the relative humidity of the air (during cooling, mist, fog, or rain) will hydrate the dried-out

anhydrous salt, which will lead to volume expansion and therefore pressure on the walls of the pores (pressure of hydration). Last, the differential behaviour of the hydration expansion pressure of gypsum, basanite, and anhydrite and between hydrous and anhydrous sulfates leads to various degradation patterns in the building materials (cracking, flaking, and powdering).

Finally, all kinds of salts could react with climatic changes and environmental conditions to add more cycles of dissolution and crystallization processes. For instance, efflorescence on the temple walls could be formed by rainwater or water vapor, and these salts can be dissolved and recrystallized into the porous system and cause more decay for the building materials.

## Conclusions

For the determination of the construction materials and their alterations, a series of multi-analytical, microscopic examinations and site investigation was carried out. The main construction material of the temple is limestone from Minia quarries. Lime gypsum joint mortar from Ramses II eras and hydraulic lime mortar from Emperor Nero were used as structural joint materials. Significantly, the research found that gypsum was added to lime as a second additive to enhance the mechanical and physical strength of the mortar. Furthermore, microcline and sepiolite were added as pozzolans to improve the resistance and durability of the Roman structural mortar, especially against water.

Salt weathering mainly causes the damage and decay of Nero's Temple. Different water sources (agricultural, wastewaters, and canals water) carried different kinds of soluble salts (chlorides, sulfates, carbonates, bicarbonates, phosphates, and nitrates), which were detected by mineralogical and elemental analysis. These salts led to the reduction of the durability and resilience of the temple building materials. Halite is considered the main decay salt that played an important role in the chemical weathering of the building materials and led to efflorescence and sub-florescence as the most dominant decay patterns in the temple construction materials. The scanning electron microscope with EDS revealed cubic and massive phases of sodium chlorides that covered the stone surfaces and created a very thick crust layer. Double Ca, Mg, and K sulfates salts (humberstonite and ungematchite) are considered the second key to salt weathering after chlorides. SEM images showed these double salt phases were in a grey dark crust over the surfaces.

Moreover, three phases of calcium sulfates (gypsum, bassanite, and anhydrite) were found in most of the samples. These salts contributed to the salt weathering of

the temple construction materials as well. The dehydration of gypsum to bassanite and anhydrite is considered the critical point for the degradation of stone and mortar surfaces. SEM images presented a significant amount of gypsum and anhydrite nodules over the construction surfaces of the temple. Phosphate salts (brushite and strengite) were detected and probably they came from irrigation water and wastewaters as precipitated on and behind the construction materials. Accordingly, materials deformations, pores, flaking, granular disintegration, loss of material, and erosions were observed by scanning electron microscope and digital microscope as a result of salt weathering and repeated cycles of dissolution and precipitation for the salts on construction materials.

Finally, the research was conducted on the salt decay for the construction materials of Nero's Temple and an assessment of the current state of preservation of this important monument. However, future studies will be needed to carry out soil studies for Nero's Temple. In addition, an urgent restoration plan should be executed to restore and preserve the remaining structural and architectural elements starting from fine (surface cleaning, salt removal, and consolidation) to geostructural (soil enhancement, columns repairs, blocks re-joining, and replacement) restoration to be kept as a world heritage monument.

#### Acknowledgements

A. Fahmy acknowledges UGEA-PHAM at University of Cadiz for carrying out the main part of the archaeometrical analysis. XRD, mXRF and SEM-EDX analysis were carried in the SCICYT of the University of Cadiz. E. Molina Piernas acknowledges co-funding from the European Social Fund (D1113102E3) and Junta de Andalucía.

#### Author contributions

AF, EMP, JML, and SDB contributed to the conception and design of this study. AF, EMP, and SDB carried out the laboratory tests. AF wrote the first draft of the manuscript. EMP, JML, and SDB contributed to the discussion of the results and collaborated in the writing of the different sections of the manuscript. EMP and SDB contributed to the funding acquisition. All authors contributed to the review of the manuscript. All authors read and approved the final manuscript.

#### Funding

The authors confirm that A. Fahmy is not currently in receipt of any research funding relating to the research presented in this manuscript.

#### Availability of data and materials

Data sharing is not applicable to this article, as no datasets were generated or analyzed during the current study.

#### Declarations

##### Competing interests

The authors declare that they have no competing interests.

##### Author details

<sup>1</sup>Department of Earth Sciences, Faculty of Sciences, University of Cadiz, Campus Río San Pedro, 11510 Puerto Real, Spain. <sup>2</sup>Conservation Department, Faculty of Archaeology, Cairo University, Giza 12613, Egypt.

Received: 19 May 2022 Accepted: 27 July 2022  
Published online: 05 August 2022

#### References

1. Ahmed AA, Fogg GE. The impact of groundwater and agricultural expansion on the archaeological sites at Luxor, Egypt. *J Afr Earth Sci*. 2014;95:93–104. <https://doi.org/10.1016/j.jafrearsci.2014.02.007>.
2. Aly N, Heras MG, Hamed A, Buergo MA, Soliman F. The influence of temperature in a capillary imbibition salt weathering simulation test on Mokattam limestone. 2015;65(317). <https://materconstrucc.revistas.csic.es/index.php/materconstrucc/article/view/1682>
3. Aly N, Hamed A. The impact of salt crystallization on the building stones of Al-Azhar Mosque. 2020;11(4):895–904. [https://ijcs.ro/public/IJCS-20-65\\_Aly.pdf](https://ijcs.ro/public/IJCS-20-65_Aly.pdf). Accessed 10 April 2022.
4. Fitzner B. Porosity properties of naturally or artificially weathered sandstones—Proc VIII International Congress on Deterioration and Conservation of Stone, Torun, 12–14 Sept 1988; 236–245.
5. Winkler M. Moisture and salts in stone. In: Stone in architecture. Springer, Berlin, Heidelberg; 1997. [https://doi.org/10.1007/978-3-662-10070-7\\_6](https://doi.org/10.1007/978-3-662-10070-7_6).
6. Benavente D, García del Cura MA, García-Guinea J, Sánchez-Moral S, Ordóñez S. Role of pore structure in salt crystallization in unsaturated porous stone. *J Cryst Growth*. 2004;260:532–44. <https://doi.org/10.1016/j.jcrysgro.2003.09.004>.
7. Moropoulou A, Labropoulos K, Konstanti A, Bakolas A. Fracture and failure of natural building stones. January 2008; vol. 53. <https://doi.org/10.1007/978-1-4020-5077-0>.
8. Cardell C, Benavente D, Rodríguez-Gordillo J. Weathering of limestone building material by mixed sulfate solutions. Characterization of stone microstructure, reaction products and decay forms. *Mater Charact*. 2008;59:1371–85. <https://doi.org/10.1016/j.matchar.2007.12.003>.
9. Brimblecombe P. Weathering of building materials. In: Urban pollution and changes to materials and building surfaces, Book Series: Air pollution reviews 2016; Vol. 5: 19–64, Imperial College Press, London
10. Oguchi CT, Yu S. A review of theoretical salt weathering studies for stone heritage. *Prog Earth Planet Sci*. 2021. <https://doi.org/10.1186/s40645-021-00414-x>.
11. Fahmy A, Molina Piernas E, Domínguez-Bella S, López JM, Helmi F. Geoenvironmental investigation Sahure's pyramid Abusir archeological site, Giza, Egypt. *Herit Sci*. 2022. <https://doi.org/10.1186/s40494-022-00699-1>.
12. Bradley SM, Middleton AP. A study of the deterioration of Egyptian limestone sculpture. *J Am Inst Conserv*. 1988;27(2):64–86. <https://doi.org/10.2307/3179403>.
13. Wu RAJ, Schlu C. The origin of soluble salts in rocks of the Thebes Mountains Egypt: the damage potential to Ancient Egyptian wall art. *J Archaeol Sci*. 2000;27:1161–72. <https://doi.org/10.1006/jasc.1999.0550>.
14. Mahmoud HM, Kantiranis N, Stratis JA. Salt damage on the wall paintings of the festival temple of Thutmosis III, Karnak Temples Complex, Upper Egypt. *Int J Environ Sci*. 2010;1(3):133–42.
15. Aboushook M, Park HD, Gouda M, Mazen O, El-Sohby M. Determination of durability of some Egyptian monument stones using digital image analysis. Proceedings of the 10th IAEG Congress—Engineering Geology for Tomorrow's Cities, Nottingham, UK, The Geological Society of London, 2006, Paper Number: 80, pp. 1–10. [https://kau.edu.sa/Files/135/Researches/59046\\_29391.PDF](https://kau.edu.sa/Files/135/Researches/59046_29391.PDF). Accessed 18 Apr 2022.
16. Navarro R, Pereira D, Fernández de Arévalo E, Sebastián-Pardo EM, Rodriguez-Navarro C. Weathering of serpentine stone due to in situ generation of calcium and magnesium sulfates. *Constr Build Mater*. 2021;280: 122402. <https://doi.org/10.1016/j.conbuildmat.2021.122402>.
17. Erić S, Matović V, Kremenović A, Colomban P, Batočanin DS, Nešković M, et al. The origin of Mg sulfate and other salts formed on pure calcium carbonate substrate—Tufa stone blocks built into the Gradac Monastery, Serbia *Constr Build Mater*. 2015;98:25–34. <https://doi.org/10.1016/j.conbuildmat.2015.08.101>.
18. Menéndez B. Estimation of salt mixture damage on built cultural heritage from environmental conditions using ECOS-RUNSALT model. *J Cult Herit*. 2017;24:22–30. <https://doi.org/10.1016/j.culher.2016.11.006>.

19. Menéndez B. Estimators of the impact of climate change in salt weathering of cultural heritage. *Geosci.* 2018. <https://doi.org/10.3390/geosciences8110401>.
20. Franzoni E. Rising damp removal from historical masonry: a still open challenge. *Constr Build Mater.* 2014;54:123–36. <https://doi.org/10.1016/j.conbuildmat.2013.12.054>.
21. Rodriguez-Navarro C, Doehe E. Salt weathering: Influence of evaporation rate, supersaturation and crystallization pattern. *Earth Surf Process Landforms.* 1999;24:191–209. [https://doi.org/10.1002/\(sici\)1096-9837\(199903\)24:3<191::aid-esp942>3e3.0.co;2-g](https://doi.org/10.1002/(sici)1096-9837(199903)24:3<191::aid-esp942>3e3.0.co;2-g).
22. Ruiz-Águdo E, Mees F, Jacobs P, Rodriguez-Navarro C. The role of saline solution properties on porous limestone salt weathering by magnesium and sodium sulfates. *Environ Geol.* 2007;52:269–81. <https://doi.org/10.1007/s00254-006-0476-x>.
23. Caruso F, Maria A, Sanchez A, Scherer GW, Flatt RJ. Chemomechanics of salt damage in stone. *Nat Commun.* 2014. <https://doi.org/10.1038/ncomms5823>.
24. Scrivano S, Gaggero L. An experimental investigation into the salt—weathering susceptibility of building limestones. *Rock Mech Rock Eng.* 2020;53(12):5329–43. <https://doi.org/10.1007/s00603-020-02208-x>.
25. Doehe E, Selwitz C, Carson D, DeTagle A. Prevention of salt damage to monuments: esem and time-lapse studies. *Microsc Microanal.* 2001;7(S2):466–7. <https://doi.org/10.1017/s1431927600028403>.
26. Lopez-Arce P, Doehe E, Martin W, Pinchin S. Sales de sulfato magnésico y materiales de edificios históricos: simulación experimental de laminaciones en calizas mediante ciclos de humedad relativa y cristalización de sales. *Mater Constr.* 2008;58:125–42. <https://doi.org/10.3989/mc.2008.v58.i289-290.77>.
27. Benavente D, de Jongh M, Cañaveras JC. Weathering processes and mechanisms caused by capillary waters and pigeon droppings on porous limestones. *Minerals.* 2021;11:1–16. <https://doi.org/10.3390/min11010018>.
28. Fitzner BJ. Investigation of weathering damage on stone monuments. *Geonomos.* 2016. <https://doi.org/10.18285/geonomos.v24i2.835>.
29. Kamh GME, Koltuk S, Ismael H. Refinement of categorization and scaling of weathering-related damage to natural stone: case study on oolitic limestone from El-Shatbi Tombs (Egypt). *Bull Eng Geol Environ.* 2017;76:39–57. <https://doi.org/10.1007/s10064-016-0946-7>.
30. Doehe E, Selwitz C, Carson D, DeTagle A. Damage to monuments from the crystallization of mirabilite, thenardite and halite: mechanisms, environment, and preventive possibilities. *Elev Annu V M Goldschmidt Conf.* 2001;1:3212.
31. Doehe E. Salt weathering: a selective review. *Geol Soc Spec Publ.* 2002;205:51–64. <https://doi.org/10.1144/GSL.SP.2002.205.01.05>.
32. Heinrichs K, Fitzner B. Stone monuments of the Nemrud Dag sanctuary/Turkey petrographical investigation and diagnosis of weathering damage. *Zeitschrift Der Dtsch Gesellschaft Für Geowissenschaften.* 2007;158:519–48. <https://doi.org/10.1127/1860-1804/2007/0158-0519>.
33. Hemeda S, Fahmy A, Sonbol A. Geo-environmental and structural problems of the first successful true pyramid, (Snefru Northern Pyramid) in Dahshur, Egypt. *Geotech Geol Eng.* 2019;37(4):2463–84. <https://doi.org/10.1007/s10706-018-00769-x>.
34. Leclant J. Revue Archéologique. 1962. 2022 Jun 25;1:115–20. <http://www.jstor.org/stable/41754847>.
35. Bailey DM, Davies WV, Spencer AJ. British Museum expedition to Middle Egypt: Ashmunein (1980), British Museum Occasional Paper 19982; 37, London.
36. Harrell JA, Storemyr P. Ancient Egyptian quarries—an illustrated overview. 2009; 7–50. [https://www.ngu.no/upload/Publikasjoner/Special%20publication/SP12\\_s7-50.pdf](https://www.ngu.no/upload/Publikasjoner/Special%20publication/SP12_s7-50.pdf). Accessed 22 Apr 2022.
37. Hemeda S, Fahmy A, Moustafa A, El HMA. The Early Basilica Church, El-Ashmonein Archaeological Site, Minia, Egypt: geo-environmental analysis and engineering characterization of the building materials. *Open J Geol.* 2019;09:157–86. <https://doi.org/10.4236/ojg.2019.93011>.
38. Fakhry M. Temples of Minia in Nero era 54–68AD, Doctoral thesis, department of archaeology (Greco-Roman), Faculty of arts, Minia University. 2015.
39. Moneim AAA, Fernández-Álvarez JP, Abu El Ella EM, Masoud AM. Groundwater management at West El-Minia Desert Area, Egypt using numerical modelling. *J Geosci Environ Prot* 2016;04:66–76. <https://doi.org/10.4236/gep.2016.47008>.
40. Abdel-Mageed Y, Hassan H, Abdel-Rahim A, Abd EL-Azeim M, Matouk M. Evaluation of groundwater quality for irrigation and its effects on some soil chemical properties in the Western Desert of El-Minia Governorate, Egypt. *J Soil Sci Agric Eng* 2018;9:283–94. <https://doi.org/10.21608/jssae.2018.35872>.
41. El-Deeb H, El Rawy M, Habib E. Water resources management: case study of El Minia Governorate, Egypt. *Int J Sci Eng Res* 2015;6.
42. <https://weather-and-climate.com/average-monthly-Rainfall-Temperature-Sunshine,al-minya-eg,Egypt>. Accessed 12 Apr 2022.
43. Spencer AJ, Bailey DM. Excavations at El-Ashmunein. Published for the Trustees of the British Museum by British Museum Publications 1983; London.
44. Whitney DL, Evans BW. Abbreviations for names of rock-forming minerals. *Am Mineral.* 2010;95:185–7. <https://doi.org/10.2138/am.2010.3371>.
45. Gunasekaran S, Anbalagan G, Pandi S. Raman and infrared spectra of carbonates of calcite structure. *J Raman Spectrosc.* 2006;37:892–9. <https://doi.org/10.1002/jrs.1518>.
46. Vitti P. Mortars and masonry—structural lime and gypsum mortars in antiquity and middle ages. *Archaeol Anthropol Sci.* 2021; <https://doi.org/10.1007/s12520-021-01408-y>.
47. Caro S. An investigation of Roman mortar technology through the petrographic analysis of archaeological material. *Constr Build Mater.* 2008;22:1807–11. <https://doi.org/10.1016/j.conbuildmat.2007.05.003>.
48. Young D. Salt attack and rising damp: a guide to salt damp in historic and older buildings. Heritage council of NSW. Heritage Victoria. South Australian Department for environment and heritage. Adelaide city council. November 2008; P. 4. ISBN 978-0-9805126-5-6. [https://cdn.environment.sa.gov.au/environment/docs/saltdamp\\_techguide.pdf](https://cdn.environment.sa.gov.au/environment/docs/saltdamp_techguide.pdf) Accessed 07 Apr 2022.
49. Derluyn H, Dewanckele J, Boone MN, Cnudde V, Derome D, Carmeliet J. Crystallization of hydrated and anhydrous salts in porous limestone resolved by synchrotron X-ray microtomography. *Nucl Instrum Methods Phys Res Sect B Beam Interact with Mater Atoms.* 2014;324:102–12. <https://doi.org/10.1016/j.nimb.2013.08.065>.
50. Vaniman DT, Martínez GM, Rampe EB, Bristow TF, Blake DF, Yen AS, et al. Gypsum, bassanite, and anhydrite at Gale crater. *Mars Am Mineral.* 2018;103:1011–20. <https://doi.org/10.2138/am-2018-6346>.
51. Balboni E, Espinosa-Marzal RM, Doehe E, Scherer GW. Can drying and rewetting of magnesium sulfate salts lead to damage of stone? *Environ Earth Sci.* 2011;63:1463–73. <https://doi.org/10.1007/s12665-010-0774-1>.
52. Gázquez F, Rull F, Medina J, Sanz-Arranz A, Sanz C. Linking groundwater pollution to the decay of 15th-century sculptures in Burgos Cathedral (northern Spain). *Environ Sci Pollut Res.* 2015;22:15677–89. <https://doi.org/10.1007/s11356-015-4754-6>.
53. Thickett D, Stanley B. Management of sodium sulfate damage to polychrome stone and buildings. 4th International conference on salt weathering of buildings and stone sculptures management. 2017;135–142. <https://www.englishheritage.org.uk/siteassets/home/learn/conversation/collections-advice-guidance/management-of-sodium-sulphate-damage-to-polychrome-stone-and-buildings.pdf>. Accessed 08 Apr 2022.
54. Rodriguez-Navarro C, Doehe E, Sebastian E. How does sodium sulfate crystallize? Implications for the decay and testing of building materials. *Cem Concr Res.* 2000;30(10):1527–34. [https://doi.org/10.1016/S0008-8846\(00\)00381-1](https://doi.org/10.1016/S0008-8846(00)00381-1).
55. Steiger M, Charola AE, Sterflinger K. Weathering and deterioration. In: Siegesmund S, Snethlage R. Stone in architecture. Springer, Berlin, Heidelberg; 2014. [https://doi.org/10.1007/978-3-642-45155-3\\_4](https://doi.org/10.1007/978-3-642-45155-3_4).
56. Gonçalves TD, Rodrigues JD, Abreu MM, Esteves AM, Silva AS. Causes of salt decay and repair of plasters and renders of five historic buildings in Portugal. *Proceedings of the International Conference on Heritage, Weathering and Conservation.* 2006; 1: 273–284.
57. Shahid SA. Developments in soil salinity assessment, modeling, mapping, and monitoring from regional to submicroscopic scales. In: Shahid SA, Abdelfattah MA, Taha FK, editors. *Developments in soil salinity assessment and reclamation.* Dordrecht: Springer Netherlands; 2013. p. 3–43. [https://doi.org/10.1007/978-94-007-5684-7\\_1](https://doi.org/10.1007/978-94-007-5684-7_1).
58. Onac BP, Sumrall J, Mylroie JE, Kearns JB. Cave Minerals of San Salvador Island, Bahamas Cave Minerals of San Salvador Island, Bahamas. 2009.

- [https://www.researchgate.net/publication/241834538\\_Cave\\_Minerals\\_of\\_San\\_Salvador\\_Island\\_Bahamas](https://www.researchgate.net/publication/241834538_Cave_Minerals_of_San_Salvador_Island_Bahamas) Accessed 08 Apr 2022.
- 59. Valsami-Jones E. Mineralogical controls on phosphorus recovery from wastewaters Mineralogical controls on phosphorus recovery from wastewaters. *Mineral Mag.* 2014. <https://doi.org/10.1180/002646101317018433>.
  - 60. Siedel H, Plehwe EV, Leisen H. Salt load and deterioration of sandstone at the temple of Angkor Wat, Cambodia. 11th International Congress on Deterioration and Conservation of Stone, Torun, Poland 2008. Proceedings, I(August), pp 267–274.
  - 61. Fernandez SP. Factors influencing salt-induced weathering of building sandstone. P44. RobertGordon University. 1999; PhD thesis. <https://openair.rgu.ac.uk>. Accessed 16 May 2022.
  - 62. Ballirano P, Melis E. Thermal behaviour and kinetics of dehydration of gypsum in air from in situ real-time laboratory parallel-beam X-ray powder diffraction. *Phys Chem Miner.* 2009;36:391–402. <https://doi.org/10.1007/s00269-008-0285-8>.
  - 63. Stambolov T, Van Asperen De Boer JRJ. The deterioration and conservation of porous building materials in monuments. A preliminary review. International centre for the study of the preservation and restoration of cultural property 1967, Stampatopresso it laboratori tipico-litografici codella DAPCO s.r.l. ViaDandolo, 8 - 00153 ROMA, Second enlarged edition. [https://www.iccrom.org/sites/default/files/2018-02/1976\\_stambolov\\_deterioration\\_eng\\_21362\\_light.pdf](https://www.iccrom.org/sites/default/files/2018-02/1976_stambolov_deterioration_eng_21362_light.pdf). Accessed 10 May 2022.

## Publisher's Note

Springer Nature remains neutral with regard to jurisdictional claims in published maps and institutional affiliations.

Submit your manuscript to a SpringerOpen® journal and benefit from:

- Convenient online submission
- Rigorous peer review
- Open access: articles freely available online
- High visibility within the field
- Retaining the copyright to your article

Submit your next manuscript at ► [springeropen.com](http://springeropen.com)